Acta Polytechnica **64**(2):77–86, 2024
https://doi.org/10.14311/AP.2024.64.0077

PARAMETRIC OPTIMISATION OF LASER WELDING OF STAINLESS STEEL 316L

Adnan Qayyum Butt[a,*], Qanita Tayyaba[a], Muhammad Ali Raza[a], Abdul Rehman[a,b], Tayyab Ali Khan[a], Muhmmad Shahzad[a,c]

[a] *Pakistan Institute of Nuclear Science and Technology, Materials Division, Pakistan*

[b] *Tsinghua University, School of Materials Science and Engineering, Key Laboratory of Advanced Materials of Ministry of Education, 100084 Beijing, China*

[c] *Clausthal University of Technology, Institute of Materials Science & Engineering, Agricolastr. 6, 38678 Clausthal-Zellerfeld, Germany*

[*] corresponding author: adnanbutt292@gmail.com

Abstract. This paper presents numerical and experimental studies focused on the optimisation of laser welding parameters for AISI 316L stainless steel. The focus of the numerical studies was to obtain the mathematical model with the least time complexity and the highest fidelity. Based on the comparison of different mathematical models, a combination of two models, double ellipsoidal and conical models, was found to be optimal for the numerical simulation of the laser welding process. The studies were also complemented by material characterization studies for validation purpose. A pulse duration of 8 milliseconds and a current of 400 amperes with an average power of 380 W were found to be the optimum parameters for laser welding of standard gauge 12 sheet of stainless steel AISI 316L. In addition, the effect of duty factor of the pulsed laser beam on the weld profile was also investigated and was found to be a major contributor to the optimisation process. The properties of the sample welded with the optimised set of parameters were also compared with the base metal, and based on the mechanical characterisation studies, it was found that the yield strength and hardness of the welded sample were improved, but the overall ductility was slightly reduced as compared to the base metal. The average weld zone size was also reduced by increasing the power density due to multiple reflections of the beam.

Keywords: FEM (Finite Element Method), FWHM (Full Width Half Maxima), PWM (Pulse Width Modulation), HAZ (Hear Affected Zone).

1. Introduction

Austenitic stainless steel is widely used in various industrial structures due to its remarkable thermo-mechanical properties [1–5]. Welding is the most widely used process for joining stainless steel structures. Laser beam welding is a superior welding technique as compared to conventional welding techniques including the TIG welding process due to its smaller fusion zone (FZ) and heat affected zone (HAZ) [3, 4, 6–8]. Laser welding, just like electron beam welding, is a high energy density welding process that can be used to join metals with thick sections. Although both of these techniques produce smaller HAZ sizes, the requirement for vacuum in electron beam welding restricts its utilization in a number of industries. For this reason, laser beam welding is considered as the preferred non-conventional welding process due to its higher quality, high speed, flexibility of input parameters, and strength of welded structures [9]. In addition, laser welding is considered to be a superior metal joining process for fusion reactor operations [10]. The importance of laser welding is increasing tenfold in industry due to the higher spectrum of energy available in laser welding operations [11]. Because of the significance of this welding process, a substantial research is being conducted to determine the most suitable input parameters for laser welding processes.

In order to model the behaviour of the parts being welded, there has been extensive research into the use of finite element methods to model the shape and size of the welds based on the thermal mapping observed during laser welding [12, 13]. The use of laser welding in practical applications requires the integration of the experimental and numerical calculations to optimally model the parameters suitable for laser welding [14].

Laser welding can be broadly classified into two major categories based on the behaviour of the incident laser beam, i.e. pulsed laser beam and continuous beam [15]. There are several parameters that influence the quality of laser welded materials. These parameters are referred to as the input parameters, which determine the behaviour of the laser welding process [16]. Laser beam diameter, laser power, interaction time, pulse width, and frequency of the incident radiation are the most important input parameters for a laser welding process [17]. Amongst all these parameters, the influence of pulse width is substantially more prominent than any other parameter for

Sample Identification	Current [A]	Pulse Width [ms]	Frequency [Hz]	Feed of Laser torch [mm/min]	Regimes	Remarks
LZ 1	250	11	4	30	Conduction Regime	Both Side Weld
LZ 2	300	11	4	30	Conduction Regime	Both Side Weld
LZ 3	350	8.0	4	30	Conduction Regime	Both Side Weld
LZ 4	400	8.0	4	30	Keyhole Regime	Both Side Weld
LZ 5	450	6.0	4	30	Keyhole Regime	Both Side Weld

Table 1. Laser welding input parameters used for this study.

pulsed laser beams [18]. Similarly, the wavelength of the laser light also plays a crucial role in terms of power absorption, and it must be carefully chosen to achieve a greater efficiency in the laser welding process. A comparison of laser welding using different wavelengths has shown that the shorter wavelength laser beams, i.e. Nd: YAG compared to CO_2, are more suitable for situations where the workpiece is a metallic material with a higher surface reflectivity, such as stainless steels [19]. Furthermore, to achieve consistent results of the laser welding process, the angle of incident laser beam also needs consideration along with other input parameters because this can also affect the weld profiles and the depth of the weld [20].

Given the unprecedented advantages associated with the laser welding operation, much research is being carried out to optimise the input parameters for various materials including magnesium alloys [21] and aluminium alloys [22]. In addition, laser welding of high entropy alloys is also being considered due to the exponential increase in the use of these materials in industry [23]. Furthermore, extensive research is also being carried out on the joining of dissimilar metals by laser welding, focusing the effects of laser beam pulse width on laser welding of dissimilar metals [24].

Along with all the input parameters of the welding process required for mathematical models [25], changes in material properties like melting and vaporisation temperatures also play a significant role in the depth of the welding penetration, the width of the bead depends on the material's reflectivity for the beam which should be taken into account in numerical studies of laser welding operations [26]. There can also be various configurations in which the laser welding can be performed, such as welding of thin sheets [27] and welding of plates attached in a butt joint configuration [28]. Based on these studies, it was found that increasing the power density of the laser beam decreases the size of the heat affected zone due to multiple reflections of the beam with the metal inside the fusion zone.

Because of the widespread usage of gauge 12 (2.7 mm thickness) stainless steel sheets of AISI 316L, this paper provides an insight into the optimal set of parameters that can be used to perform laser welding of these sheets joined in a butt joint configuration using both the experimental and numerical methods. Using the concepts developed in this paper, the sheets of different materials can also be welded with their respective parameters. This paper can be broadly classified into two sections. In the first part, different mathematical models were compared and numerical calculations were performed on a stainless steel sheet with the given configuration. The numerical studies were used to evaluate thermal mapping along the thickness of the sheet to capture the details of the thermal gradient. Furthermore, the optimised mathematical model was used to model the pattern observed on the surface of the metal. The numerical calculations were complemented with the experimental investigation for the validation of the results obtained from the numerical studies. The experimental studies were performed on plates joined using Nd:YAG source. Material characterisation techniques, including mechanical characterisation and fractographic investigations, were used to determine the optimum set of parameters for welding plates joined in a butt joint configuration. Based on the results of the numerical investigation, it was concluded that the double ellipsoidal model is better suited for lower power densities, while the conical model is optimal for operations performed at higher power densities. Therefore, to obtain high-fidelity models for laser welding with minimum time complexity, it is important to have a combination of the models based on the energy density of the incident laser beam.

2. Experimental setup

In this study, pulsed Neodymium-Doped Yttrium Aluminium Garnet (Nd:YAG) laser welding system was used for welding of stainless steel AISI 316L. Sheets of 2.7 mm thickness (gauge number 12) were joined in a butt joint configuration. The machine used for this operation had a peak power of 600 W and a maximum average power of 500 W. The conical focal length of the machine is 175 mm and the spot size diameter of the weld is 300 µm. Because of the issues associated with the keyhole regime's instabilities, the welding was done on both sides of the samples to ensure a proper joint without facing the issues of localised vaporisation of materials caused by a higher power of the beam. A pulsed laser mode was used for the welding. A summary of the main welding parameters used for this study is given in Table 1.

3. Results and discussion

The weld profile along the thickness is analogous to the thermal mapping along the thickness of the weld which can be modelled using the heat source equation. The basic mathematical model used to capture the details of the temperature distribution and heat diffusion is governed by equation:

$$\frac{\partial}{\partial x}\left(K(T)\frac{\partial T}{\partial x}\right)+\frac{\partial}{\partial y}\left(K(T)\frac{\partial T}{\partial y}\right) +\frac{\partial}{\partial z}\left(K(T)\frac{\partial T}{\partial z}\right)+Q=\rho(T)C_p(T)\frac{\partial T}{\partial t}, \tag{1}$$

where

T indicates the temperature,

$K(T)$ is the thermal conductivity,

$\rho(T)$ is the density,

$C_p(T)$ is the specific heat,

Q is the volumetric heat flux.

The terms on the right account for the transient response of the system. Since in the case of welding, there are both the convection and radiation phenomena, the the governing equations used for this case are:

$$q_c = \rho(T)h_c\Delta T, \tag{2}$$

$$q_r = \varepsilon\sigma(T^4 - T_o^4), \tag{3}$$

where

q_c is the convective heat flux,

q_r is the radiative heat flux in these equations.

For welding processes such as laser welding, radiation becomes the main source of heat and convection serves as heat sink. From experimental results of welded samples and from literature, it is clear that the weld profile changes directly as the temperature profile changes.

The main input parameters for laser welding are welding current, pulse width, frequency, and welding speed, as these directly affect the energy density of a pulsed laser beam used in the pulsed laser welding process, and since the energy density has a direct relationship to all of these parameters [29–31] therefore the power output for the case of this study would be determined by the peak power and pulse width of the beam.

The magnitude of the laser power density on the workpiece determines the behaviour of the incident laser beam. A power density in the range of $10^6\,\mathrm{W\,cm^{-2}}$ causes melting, whereas a higher power density of $10^7\,\mathrm{W\,cm^{-2}}$ causes boiling, resulting in material loss, which is used for laser cutting [32]. For lower power densities with the characteristic behaviour of the conduction regime, the welding heat source can best be fitted using the double ellipsoid model [33]. The model can be described by equation:

$$q(x,y,z,t)=\frac{6\sqrt{3}fQ}{abc\pi\sqrt{\pi}}e^{-\frac{3x^2}{a^2}} e^{-\frac{3y^2}{b^2}}e^{-\frac{3[z+v(\tau-t)]^2}{c^2}}, \tag{4}$$

where Q is the input power given by equation:

$$Q = 2\eta VI, \tag{5}$$

where

η is the efficiency of the heat source,

V is the voltage,

I is the current.

In the double ellipsoid equation, v is the velocity, τ is the lag factor, t is the computational time, and f is the fraction whose value is dependent on the quadrant. For the front and rear quadrants, the symbols are indicated as f_f and f_r, respectively. Since the main input parameter for this study is the welding current, which, being a pulsed wave, is directly related to the full width at half maximum (FWHM). By combining the FWHM with the pulse width modulation (PWM), the heat generated by the pulsed wave can be calculated. Increasing the pulse width results in higher values of PWM and the same trend is observed for the magnitude of the current. For the case of this study, the duty of the pulse can be calculated using the formula:

$$\text{Duty cycle} = \frac{t_{\text{on}}}{t_{\text{on}}+t_{\text{off}}} = \frac{t_{\text{on}}}{T}, \tag{6}$$

where

t_{on} is the pulse width,

T is the time period of the wave given by the formula:

$$T = \frac{1}{f}. \tag{7}$$

Since frequency f is 4 Hz, T is 250 ms. Therefore, the parameters for the laser welding process are given in Table 2.

Peak power and average power are given by equations:

$$\text{Average power} = \frac{E}{T}, \tag{8}$$

$$\text{Peak power} = \frac{E}{t_{\text{on}}}. \tag{9}$$

For power densities greater than conduction regimes, the double ellipsoidal model does not capture the details associated with the multiple reflections of the laser beam inside the fusion zone of the weld [26]. For welding operations performed at higher power densities, an extension of the original Goldak double ellipsoidal model can be used, which can also incorporate

Sample	LZ-1	LZ-2	LZ-3	LZ-4	LZ-5
Duty cycle	4.4 %	4.4 %	3.2 %	3.2 %	2.4 %
Average Power [W]	200	260	320	380	440
Peak Power [W]	4 545	5 909	10 000	11 875	18 333

Table 2. Duty cycle of laser beam based on the pulse width of the beam.

the conical portion of the weld profile. The mathematical model uses the double ellipsoid and conical heat power density model [34]. The equation used for this model is given by equation:

$$q(x,y,z,t) = \frac{6R_{\mathrm{de}}\sqrt{3}fQ}{abc\pi\sqrt{\pi}S} e^{-\frac{s(x-b_g)^2}{a^2}} e^{-\frac{s(y-d_g)^2}{b^2}} e^{-\frac{s[z+v(\tau-t)]^2}{c^2}} \forall y \geq d_g, \tag{10}$$

where R_{de} is the factor that can be divided into 2 parts, depending on the quadrant. For rear and front quadrant, the factor is represented as R_{rde} and R_{fde}, respectively. As this is an extension of the original model, the conical model embedded in the double ellipsoidal model is enforced using the equation:

$$q(x,y,z,t) = \frac{54R_{\mathrm{conical}}e^3Q}{\pi^2(e^3-1)SS_q(d_g-y_i)} e^{-\frac{s(x-b_g)^2}{(\lceil a)^2}} e^{-\frac{s[z+v(\tau-t)]^2}{(\lceil c)^2}} \forall y \geq d_g, \tag{11}$$

where

$\lceil a = a - ((a - ai)(d_g - y)/(d_g - y_i)),$

$\lceil c = c - ((c - ci)(d_g - y)/(d_g - y_i)).$

Both the transitional and keyhole regimes can be accurately described from the proposed mathematical model. The flaw of this model is the associated time complexity. To compensate for the time complexity of this model, a simpler conical model designed specifically for higher power densities was adopted to capture the details of the weld profile [35]. The conical heat distribution model uses linear interpolation for the temperature profile and is given by equations:

$$q(x,y,z,t) = Q\,exp\left(\frac{x^2+y^2}{r_0^2}\right), \tag{12}$$

$$r_0 = r_e + \left(\frac{r_i + r_e}{z_i - z_e}\right)(z - z_e). \tag{13}$$

The temperature distribution derived using the Goldak double ellipsoidal model for conduction regime and the conical model for keyhole regime are shown in Figure 1 and Figure 2, respectively. It is pertinent to mention that the conical model fails to predict the response in the case of lower power densities [36], therefore, considering the wide range of power densities available in the laser welding process, it is important to consider the regime in which the temperature distribution falls in order to have a higher fidelity of the proposed mathematical model.

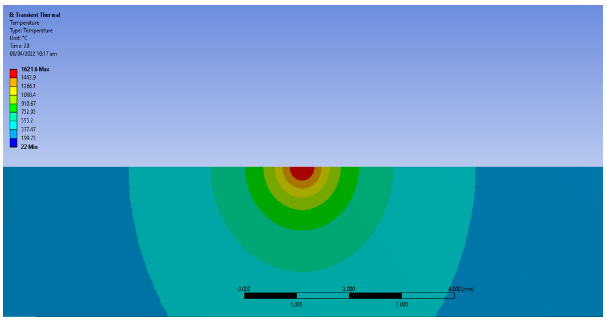

Figure 1. FEM results of the Goldak Double Ellipsoid Model.

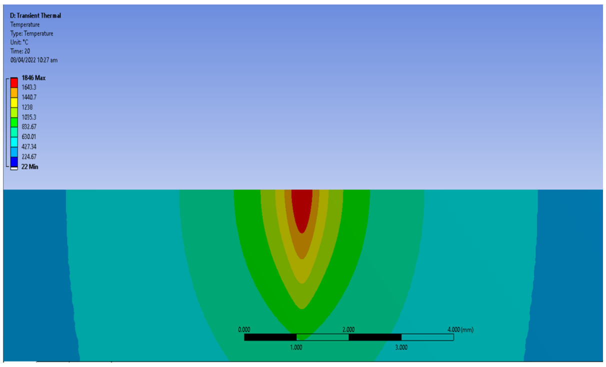

Figure 2. FEM results of Conical Model.

The microstructure of the weld-zone for welded sheets of stainless-steel with various welding input parameters is given in Figure 3. The laser power has a direct influence on the size of the heat affected zone, which can clearly be seen in the microstructure of the welded plates. Increasing the power density changes both the dimensions and morphology of the obtained weld structure [37].

The microstructures of the welded sheets can be used to estimate the size of the weld zone, which is shown in Table 3 for all the different weld conditions.

From these results, it is clear that as the power of the laser beam increases, the width of the weld zone decreases due to the multiple reflections of the beam inside the fusion zone [26]. It is also important to consider here that the influence of the duty cycle is more prominent than peak power.

The changes in the microstructure within the heat affected zone on the surface of the sheet is shown in Figure 4. The dark coloured contours on the microstructures define the boundaries of heat affected zone. It can clearly be seen that the isotherms are periodically aligned along the width, indicating that

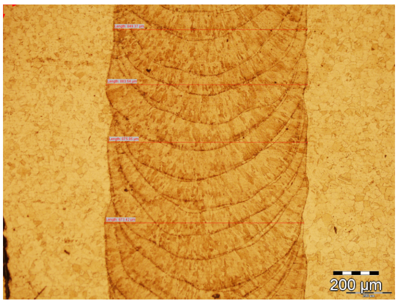

(a). LZ1.

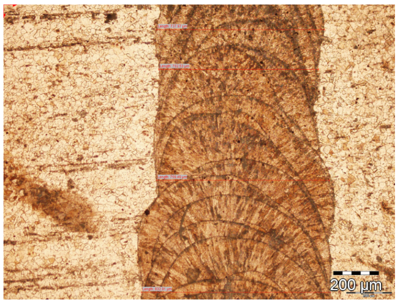

(b). LZ2.

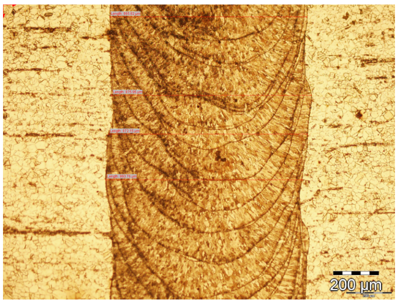

(c). LZ3.

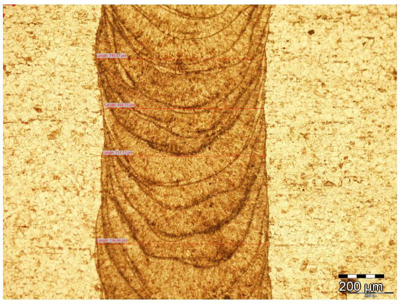

(d). LZ4.

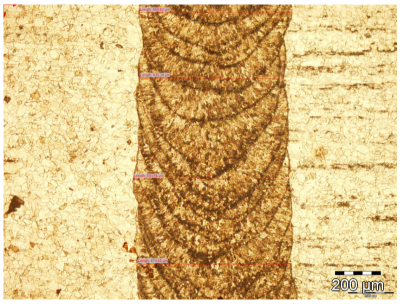

(e). LZ5.

Figure 3. Microstructure of laser welded sheet along its surface.

Sample	**LZ-1**	**LZ-2**	**LZ-3**	**LZ-4**	**LZ-5**
Average Weld-zone Size [µm]	871 ± 10	758 ± 37	869 ± 5	730 ± 15	667 ± 18

Table 3. Weld zone size for different powers of laser beam.

there is no pulse overlap causing constructive or destructive interference in the materials. In addition, the grain size increases from the centre of the weld zone towards the base metal. Based on the comparison of the grain size of the base metal, the smaller grain can be identified in the weld zone and coarser grain near the base metal. Semicircular pattern can be seen along the width of the plate in the microstructure. Another important observation is that in the heat affected zone, the grains grow from one of these semi-circles to the next semi-circle. This behaviour is attributed to the cooling cycle along the width of the plate. The semicircular patterns created along the width of the plate are considered to be the cooling isotherms which are responsible for the temperature profiles observed along the weld line [38]. These circular patterns observed during the welding process are directly influenced by power densities of incident laser beam, which directly influence the HAZ size [39]. Figure 5 also shows the results of the numerical analysis performed along the width of the plate as a function of time. To ensure proper bonding of the welded plates and to avoid any instabilities caused by the formation of localised keyhole regimes, it is also important to select an optimum travel speed of the welding beam. At lower speeds, the temperature gradient can be higher than that obtained in this study. This can result in localised vaporization on the surface. Comparing the temperature difference between the vaporisation and melting temperatures for stainless steel and that obtained from the temperature distribution along the weld line, it can be concluded that the final travel speed chosen in this paper is optimised.

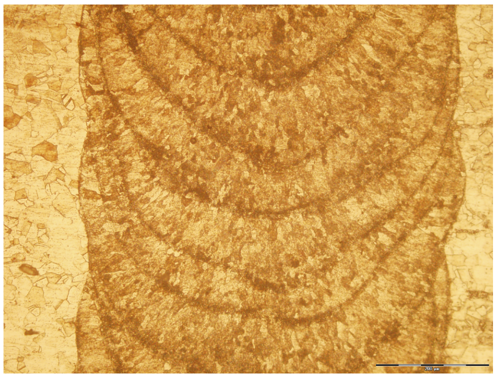

Figure 4. Isotherms in the microstructure observed on the surface of the welded sheet: Hardness of the samples observed from the centre of the weld zone to the base metal.

In terms of the application of welded sheets in any structure, it is important to quantify the response of the sheet against external stimuli. Because of the uncertainties associated with the heat affected zone, the laser welding is considered a superior welding technique due to its smaller HAZ as compared to TIG welding [40]. The microstructural features of the

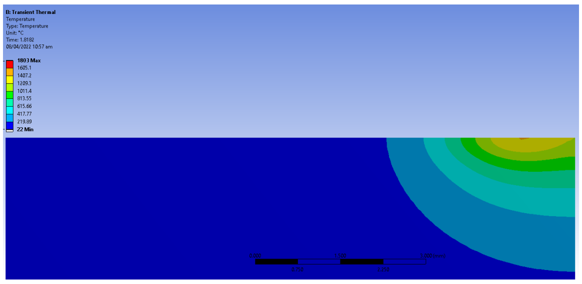

(a). 2 sec.

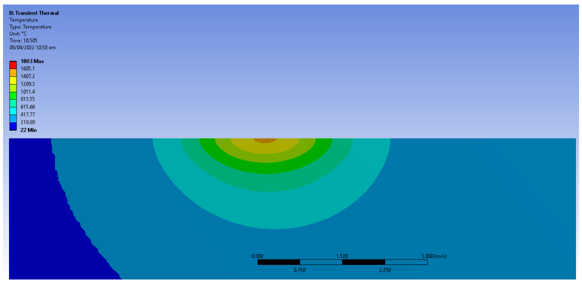

(b). 10 sec.

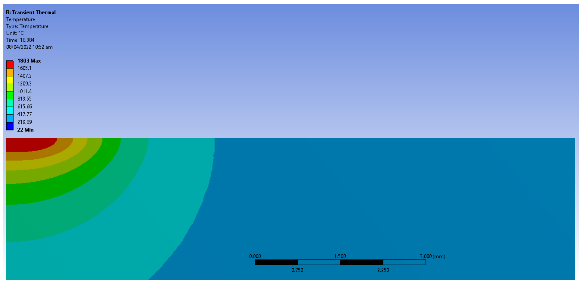

(c). 19 sec.

Figure 5. FEM analysis of the temperature profile observed along the width of the sheet at different times.

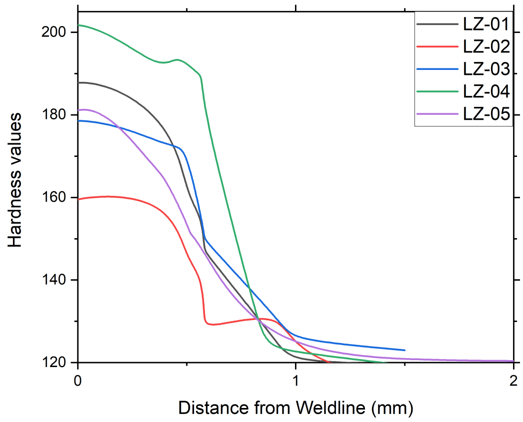

Figure 6. Vickers hardness profile along the heat affected zone on the surface from centre of the heat affected zone to the base metal.

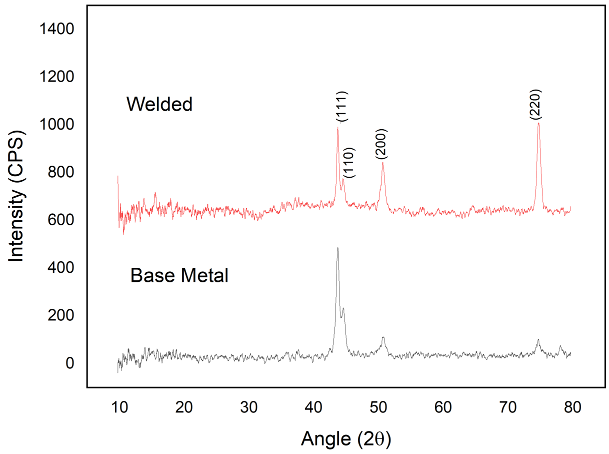

Figure 7. Comparison of XRD of the base metal and heat affected zone.

welded plates can also be linked with the mechanical response of materials [41–43].

In order to have an idea of the behaviour of the material against external loads, micro-Vickers hardness test was carried out and the variation in the hardness was observed along a line from the centre of the weld zone on the surface of the of specimen towards the base metal as shown in the Figure 4 and the results of this test are shown in Figure 6. It can be clearly seen that the hardness of each sample reaches a steady value equal to the base metal hardness after the heat affected zone.

The values of hardness were higher in the fusion zone and decreased towards the base material. This behaviour can be explained by the microstructural evolution along different isotherms as shown in Figure 4. Moreover, the most important factor, which contributes to the changes in the hardness, is the formation of secondary phases, which cause the hardness of the materials to increase.

As different cooling isotherms are observed along the hardness measurement line, the fluctuations observed along the line can be associated with the transition from one cooling isotherm to the next. Since the boundaries of the isotherms indicate the region of a lower temperature, as confirmed by the FEM analysis, and since the temperature is highest in the centre of the isotherm and decreases towards the boundaries of the isotherm, this is directly related to the morphology of the grains, which in turn dictates the hardness value. Moreover, it is evident from the hardness values that the pattern is the same for all cases. The only difference is in the peak values and the width of the variations of hardness, which can be directly linked to the energy input to the material and thus accompanying changes in the grain morphology.

XRD was also performed on the samples using a Cu Ka wavelength of 1.5418 Å to study the formation of different phases before and after the welding process. Figure 7 shows a comparison of diffraction peaks for the welded and base-metal regions of the samples. When the peaks were compared to the JCPD card number 33-0397 for 316L [44, 45], peaks of the austenitic phases were observed, i.e. (111), (200), and (220). The XRD pattern revealed that the base-metal component of the sheet has a preferential grain development along the plane

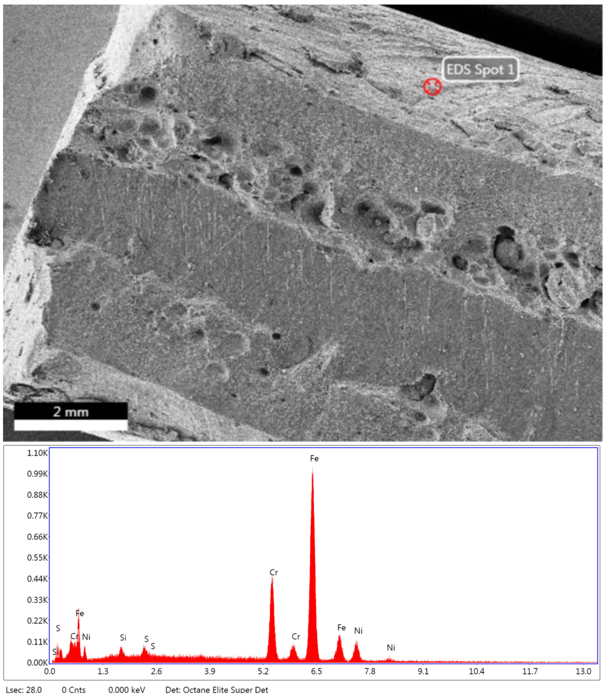

Figure 8. EDX analysis of welded area.

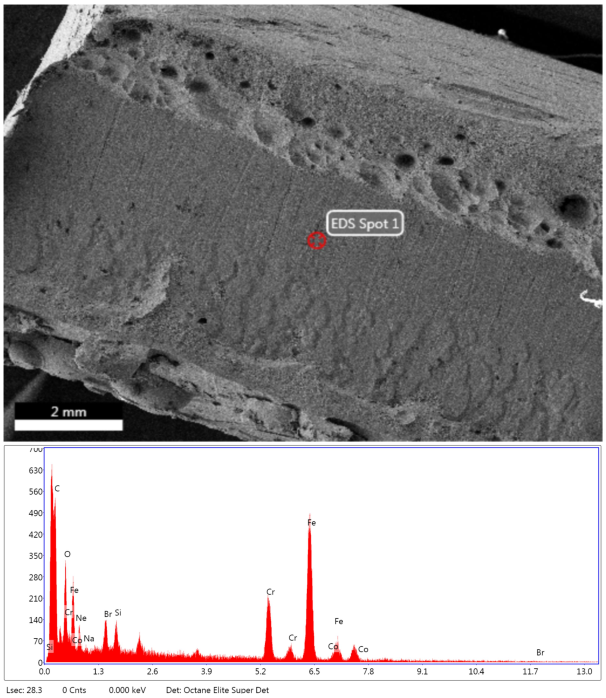

Figure 9. EDX analysis of base metal.

(111), which is the representative behaviour of rolled sheets. After the welding process, there is a random grain growth along the austenitic planes, which can be related to the fusion welding process.

The surface of all the samples were properly cleaned and the EDX analysis was also performed. The peak of carbon in the results indicate the presence of carbide, as shown in Figure 8. The presence of carbide can also be the reason for higher values of the hardness observed near the centre of the fusion zone [46, 47]. The peak in the hardness values obtained due to carbide is considered to be secondary hardness [48]. The concentration of carbide precipitates is higher in the centre due to the highest affinity for diffusion at higher temperatures in the centre of the fusion zone. The EDX comparison of the sample carried out in the middle section showed a very low carbon concentration, which is the nominal behaviour for steels as shown in Figure 9.

In order to check the strength of the weld, tensile tests were carried out on the sheets welded at various welding parameters in such a way that the tensile load was applied perpendicular to the weld with the welded section in the middle of the gauge length region. The results of the tensile tests are given in Figure 10. Laser welding is regarded as the superior welding technique based on the results of the comparison of the performance of TIG welded and laser welded materials [3]. For the tensile behaviour of welded sheets, it is important to consider the degree of weld penetration. The reason for the highest tensile strength in the case of LZ-4 was revealed by fractography of the tensile test samples shown in Figure 11. The SEM analysis of all samples revealed that samples LZ-1, LZ-2 and LZ-3

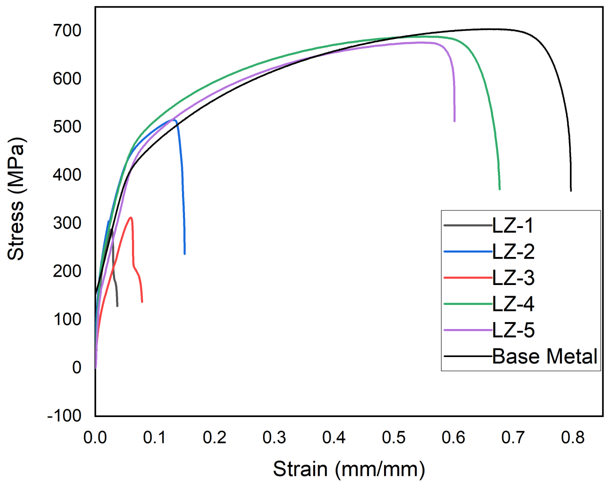

Figure 10. Tensile Tests of all samples welded with different input parameters.

have incomplete weld penetration across the thickness of the specimen. In the case of samples LZ-4 and LZ-5, there was a complete weld penetration along the thickness of the sheet. The reason for having the lower strength in the case of LZ-5 can be attributed to the welding instabilities associated with the keyhole regime. These instabilities cause detrimental effects on the strength of the welded joint [26]. Furthermore, Figure 11 reveal the presence of localised vaporisation on the surface of the weld zone in the form of discontinuous flakes on the surface, which is also one of the primary causes for the specimen to have a lower strength even with a complete weld penetration. The findings of the comparison of the sample having the highest strength and ductility with those of the unwelded sample can be used to gauge the quality of the

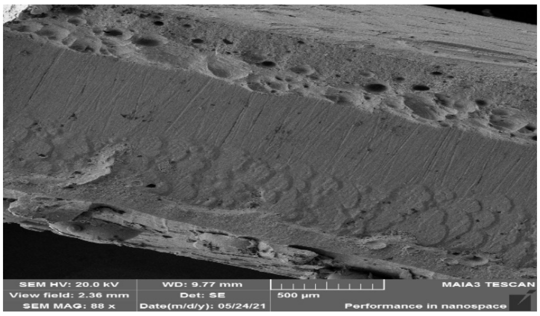

(A). LZ-1 – showing incomplete weld penetration.

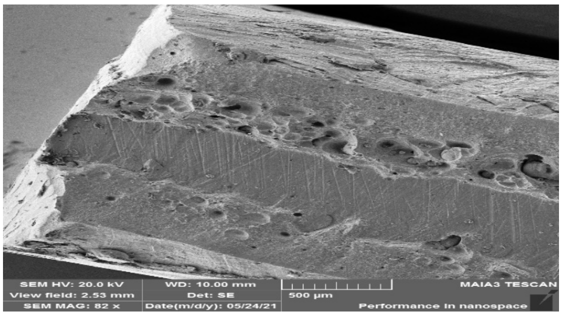

(B). LZ-3 – showing incomplete weld penetration .

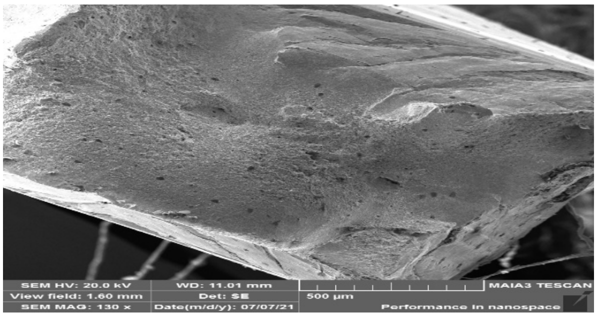

(C). LZ-4 – showing complete weld penetration .

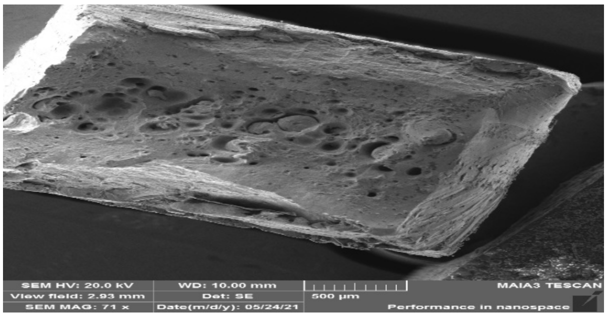

(D). LZ-5 – showing complete weld penetration with localised surface vaporisation.

FIGURE 11. SEM analysis of LZ-1, LZ-3, LZ-4 and LZ-5.

weld obtained. The presence of porosity observed in the fractographs could be a reason for the decreased strength compared to the strength of the un-welded sheets [49].

4. Conclusion

The extensive study has been carried out in relation to the welding of steel plates using both material characterisation and numerical calculations for the optimised set of input parameters for laser welding of stainless steel AISI 316L plates which can be concluded as follows:

(1.) Optimum power should be used to achieve full penetration along the thickness of the sheets being welded (LZ-4). Higher power may result in localised vaporisation (LZ-5) while lower power may result in incomplete penetration (LZ-1, LZ-2 and LZ-3).

(2.) The higher energy laser beam carries much more energy resulting in a greater number of laser beam reflections. This results in a reduction in the width of the heat affected zone at a constant pulse width (LZ-1 and LZ-2).

(3.) Reducing the pulse width results in a reduced duty factor, which directly affects the energy delivered to the welded metal. This results in a wider fusion zone as the pulse width was reduced from 11 ms to 8 ms, which is a hallmark of lower-power welding process.

(4.) The hardness profile along the heat affected zone indicated a peak in the hardness value at the centre, which is due to the grain morphology and secondary phase precipitation.

(5.) The optimum mathematical model with the least time complexity and the highest fidelity required a combination of two models i.e., double ellipsoidal and conical models. The Goldak Double Ellipsoidal Model gave a very good approximation for patterns observed at lower power densities while the conical model was found to be optimal for keyhole regimes.

References

[1] H. T. Serindağ, G. Çam. Multi-pass butt welding of thick AISI 316L plates by gas tungsten arc welding: Microstructural and mechanical characterization. *International Journal of Pressure Vessels and Piping* **200**:104842, 2022. https://doi.org/10.1016/j.ijpvp.2022.104842

[2] H. T. Serindağ, G. Çam. Characterizations of microstructure and properties of dissimilar AISI 316L/9Ni low-alloy cryogenic steel joints fabricated by gas tungsten arc welding. *Journal of Materials Engineering and Performance* **32**(15):7039–7049, 2023. https://doi.org/10.1007/s11665-022-07601-x

[3] F. S. Neto, D. Neves, O. M. M. Silva, et al. An analysis of the mechanical behavior of AISI 4130 steel after TIG and laser welding process. *Procedia Engineering* **114**:181–188, 2015. https://doi.org/10.1016/j.proeng.2015.08.057

[4] G. Çam, M. Koçak. Progress in joining of advanced materials. *International Materials Reviews* **43**(1):1–44, 1998. https://doi.org/10.1179/imr.1998.43.1.1

[5] M. Şenol, G. Çam. Investigation into microstructures and properties of AISI 430 ferritic steel butt joints fabricated by GMAW. *International Journal of*

Pressure Vessels and Piping **202**:104926, 2023. https://doi.org/10.1016/j.ijpvp.2023.104926

[6] G. Çam, M. Koçak. Progress in joining of advanced materials: Part 1: Solid state joining, fusion joining, and joining of intermetallics. *Science and Technology of Welding and Joining* **3**(3):105–126, 1998. https://doi.org/10.1179/stw.1998.3.3.105

[7] G. Çam, M. Koçak, J. dos Santos. Developments in laser welding of metallic materials and characterization of the joints. *Welding in the World* **43**:13–26, 1999.

[8] G. Çam, Ç. Yeni, S. Erim, et al. Investigation into properties of laser welded similar and dissimilar steel joints. *Science and Technology of Welding and Joining* **3**(4):177–189, 1998. https://doi.org/10.1179/stw.1998.3.4.177

[9] S. Katayama. *7 - Understanding and Improving Process Control in Pulsed and Continuous Wave Laser Welding*, pp. 153–183. Woodhead Publishing, 2018. https://doi.org/10.1016/B978-0-08-101252-9.00007-8

[10] A. Sanderson, C. S. Punshon, J. D. Russell. Advanced welding processes for fusion reactor fabrication. *Fusion Engineering and Design* **49–50**:77–87, 2000. https://doi.org/10.1016/S0920-3796(00)00407-5

[11] H. GuoMing, Z. Jian, L. JianQang. Dynamic simulation of the temperature field of stainless steel laser welding. *Materials & Design* **28**(1):240–245, 2007. https://doi.org/10.1016/j.matdes.2005.06.006

[12] M. R. Frewin, D. A. Scott. Finite element model of pulsed laser welding. *Welding Journal* **78**:15-s–22-s, 1999.

[13] N. Sonti, M. F. Amateau. Finite-element modeling of heat flow in deep-penetration laser welds in aluminum alloys. *Numerical Heat Transfer, Part A: Applications* **16**(3):351–370, 1989. https://doi.org/10.1080/10407788908944721

[14] W. S. Chang, S. J. Na. A study on the prediction of the laser weld shape with varying heat source equations and the thermal distortion of a small structure in micro-joining. *Journal of Materials Processing Technology* **120**(1):208–214, 2002. https://doi.org/10.1016/S0924-0136(01)00716-6

[15] M. Pastor, H. Zhao, T. DebRoy. Continuous wave-Nd: yttrium-aluminum-garnet laser welding of am60B magnesium alloy. *Journal of Laser Applications* **12**(3):91–100, 2000. https://doi.org/10.2351/1.521922

[16] W. J. Suder, S. Williams. Power factor model for selection of welding parameters in CW laser welding. *Optics & Laser Technology* **56**:223–229, 2014. https://doi.org/10.1016/j.optlastec.2013.08.016

[17] S. Kuo. *Welding Metallurgy*. John Wiley & Sons, Inc., Hoboken, New Jersey, 2nd edn., 2003. ISBN 0-471-43491-4.

[18] N. Kumar, M. Mukherjee, A. Bandyopadhyay. Comparative study of pulsed Nd:YAG laser welding of AISI 304 and AISI 316 stainless steels. *Optics & Laser Technology* **88**:24–39, 2017. https://doi.org/10.1016/j.optlastec.2016.08.018

[19] A. K. Dubey, V. Yadava. Experimental study of Nd:YAG laser beam machining – an overview. *Journal of Materials Processing Technology* **195**(1):15–26, 2008. https://doi.org/10.1016/j.jmatprotec.2007.05.041

[20] Y. Liao, M. Yu. Effects of laser beam energy and incident angle on the pulse laser welding of stainless steel thin sheet. *Journal of Materials Processing Technology* **190**(1):102–108, 2007. https://doi.org/10.1016/j.jmatprotec.2007.03.102

[21] L. Liu, T. Watanabe, M. Heger, et al. Contributor contact details. In *Welding and Joining of Magnesium Alloys*, pp. xi–xiii. Woodhead Publishing, 2010. https://doi.org/10.1016/B978-1-84569-692-4.50022-5

[22] A. El-Batahgy, M. Kutsuna. Laser beam welding of AA5052, AA5083, and AA6061 aluminum alloys. *Advances in Materials Science and Engineering* **2009**:974182, 2009. https://doi.org/10.1155/2009/974182

[23] Z. Chen, B. Wang, B. Duan, X. Zhang. Mechanical properties and microstructure of laser welded FeCoNiCrMn high-entropy alloy. *Materials Letters* **262**:127060, 2020. https://doi.org/10.1016/j.matlet.2019.127060

[24] P. Kumar, A. N. Sinha. Effect of pulse width in pulsed Nd:YAG dissimilar laser welding of austenitic stainless steel (304 L) and carbon steel (st37). *Lasers in Manufacturing and Materials Processing* **5**(4):317–334, 2018. https://doi.org/10.1007/s40516-018-0069-z

[25] W. K. Younis, F. A. Kasir. Total efficiency and output power of Nd:YAG laser with spatial interaction efficiency factor. *Rafidain Journal of Science* **17**(3):78–87, 2006. https://doi.org/10.33899/RJS.2006.43412

[26] L. Huang, X. Hua, D. Wu, F. Li. Numerical study of keyhole instability and porosity formation mechanism in laser welding of aluminum alloy and steel. *Journal of Materials Processing Technology* **252**:421–431, 2018. https://doi.org/10.1016/j.jmatprotec.2017.10.011

[27] V. A. Ventrella, J. R. Berretta, W. de Rossi. Pulsed Nd:YAG laser seam welding of AISI 316L stainless steel thin foils. *Journal of Materials Processing Technology* **210**(14):1838–1843, 2010. https://doi.org/10.1016/j.jmatprotec.2010.06.015

[28] J. Wang, L. Yang, M. Sun, et al. Effect of energy input on the microstructure and properties of butt joints in DP1000 steel laser welding. *Materials & Design* **90**:642–649, 2016. https://doi.org/10.1016/j.matdes.2015.11.006

[29] C. Hitz, J. Ewing, J. Hecht. *Introduction to Laser Technology*. John Wiley & Sons, Ltd., 2012. ISBN 9780470916209. https://doi.org/10.1002/9781118219492

[30] Y. F. Tzeng. Process characterisation of pulsed Nd:YAG laser seam welding. *The International Journal of Advanced Manufacturing Technology* **16**(1):10–18, 2000. https://doi.org/10.1007/PL00013126

[31] M. J. Torkamany, M. J. Hamedi, F. Malek, J. Sabbaghzadeh. The effect of process parameters on keyhole welding with a 400 W Nd:YAG pulsed laser. *Journal of Physics D: Applied Physics* **39**(21):4563, 2006. https://doi.org/10.1088/0022-3727/39/21/009

[32] J. M. William M. Steen. *Laser Material Processing*. Springer London, London, 4th edn., 2010. ISBN 978-1-84996-061-8. https://doi.org/10.1007/978-1-84996-062-5

[33] J. Goldak, M. Akhlaghi. *Computational Welding Mechanics*. Springer US, 2005. ISBN 978-0387-23287-4. https://doi.org/10.1007/b101137

[34] T. F. Flint, J. A. Francis, M. C. Smith, J. Balakrishnan. Extension of the double-ellipsoidal heat source model to narrow-groove and keyhole weld configurations. *Journal of Materials Processing Technology* **246**:123–135, 2017. https://doi.org/10.1016/j.jmatprotec.2017.02.002

[35] T. Kik. Heat source models in numerical simulations of laser welding. *Materials* **13**(11):2653, 2020. https://doi.org/10.3390/ma13112653

[36] P. Teixeira, D. Araújo, L. Cunha. Study of the Gaussian distribution heat source model applied to numerical thermal simulations of tig welding processes. *Ciencia and Engenharia/Science and Engineering Journal* **23**:115–122, 2014. https://doi.org/10.14393/19834071.2014.26140

[37] J. Meško, A. Zrak, K. Mulczyk, S. Tofil. Microstructure analysis of welded joints after laser welding. *Manufacturing Technology Journal* **14**(3):355–359, 2014. https://doi.org/10.21062/ujep/x.2014/a/1213-2489/MT/14/3/355

[38] A. Belhadj, J. Bessrour, J.-E. Masse, et al. Finite element simulation of magnesium alloys laser beam welding. *Journal of Materials Processing Technology* **210**(9):1131–1137, 2010. https://doi.org/10.1016/j.jmatprotec.2010.02.023

[39] A.-M. El-Batahgy. Effect of laser welding parameters on fusion zone shape and solidification structure of austenitic stainless steels. *Materials Letters* **32**(2):155–163, 1997. https://doi.org/10.1016/S0167-577X(97)00023-2

[40] X.-L. Gao, L.-J. Zhang, J. Liu, J.-X. Zhang. A comparative study of pulsed Nd:YAG laser welding and TIG welding of thin Ti6Al4V titanium alloy plate. *Materials Science and Engineering: A* **559**:14–21, 2013. https://doi.org/10.1016/j.msea.2012.06.016

[41] L. Zhang, X. Li, Z. Nie, et al. Comparison of microstructure and mechanical properties of TIG and laser welding joints of a new Al-Zn-Mg-Cu alloy. *Materials & Design* **92**:880–887, 2016. https://doi.org/10.1016/j.matdes.2015.12.117

[42] A. Chamanfar, T. Pasang, A. Ventura, W. Z. Misiolek. Mechanical properties and microstructure of laser welded Ti-6Al-2Sn-4Zr-2Mo (Ti6242) titanium alloy. *Materials Science and Engineering: A* **663**:213–224, 2016. https://doi.org/10.1016/j.msea.2016.02.068

[43] R. Oyyaravelu, P. Kuppan, N. Arivazhagan. Metallurgical and mechanical properties of laser welded high strength low alloy steel. *Journal of Advanced Research* **7**(3):463–472, 2016. https://doi.org/10.1016/j.jare.2016.03.005

[44] G. Silva, M. R. Baldissera, E. d. S. Trichês, K. R. Cardoso. Preparation and characterization of stainless steel 316L/HA biocomposite. *Materials Research* **16**(2):304–309, 2013. https://doi.org/10.1590/S1516-14392012005000182

[45] M. Dadfar, M. H. Fathi, F. Karimzadeh, et al. Effect of TIG welding on corrosion behavior of 316L stainless steel. *Materials Letters* **61**(11):2343–2346, 2007. https://doi.org/10.1016/j.matlet.2006.09.008

[46] J. Wang, Z. Sun, B. Shen, et al. Effects of secondary carbide precipitation and transformation on abrasion resistance of the 16Cr-1Mo-1Cu white iron. *Journal of Materials Engineering and Performance* **15**(3):316–319, 2006. https://doi.org/10.1361/105994906X108602

[47] J. Akré, F. Danoix, H. Leitner, P. Auger. The morphology of secondary-hardening carbides in a martensitic steel at the peak hardness by 3DFIM. *Ultramicroscopy* **109**(5):518–523, 2009. https://doi.org/10.1016/j.ultramic.2008.11.010

[48] D. Sorensen, B. Q. Li, W. W. Gerberich, K. A. Mkhoyan. Investigation of secondary hardening in Co-35Ni-20Cr-10Mo alloy using analytical scanning transmission electron microscopy. *Acta Materialia* **63**:63–72, 2014. https://doi.org/10.1016/j.actamat.2013.10.005

[49] V. I. Murav'ev. Problems of pore formation in welded joints of titanium alloys. *Metal Science and Heat Treatment* **47**(7):282–288, 2005. https://doi.org/10.1007/s11041-005-0068-5